Chinmo is a novel regulator of differential Hippo signaling response within a single developing organ

Shreeharsha Tarikere[1,2] *, Tarun Kumar[1,3] *, Guillem Ylla[1,4], Cassandra G. Extavour[1,3,5]

1. Department of Organismic & Evolutionary Biology, Harvard University, Cambridge MA, USA.
2. Current address: Department of Human Genetics, McGill University, Montréal, Québec, Canada
3. Howard Hughes Medical Institute, Bethesda MD, USA
4. Current address: Laboratory of Bioinformatics and Genome Biology, Faculty of Biochemistry, Biophysics and Biotechnology, Jagiellonian University, Kraków, Poland
5. Department of Molecular & Cellular Biology, Harvard University, Cambridge MA, USA

* Contributed equally

Correspondence: guillem.ylla@uj.edu.pl, extavour@oeb.harvard.edu

ABSTRACT

Orchestrated control of proliferation of multiple cell types is essential for building a healthy organ. Here we use larval ovary development in *Drosophila melanogaster* as a model to understand the homeostasis of somatic and germ line cells in the formation of the female adult reproductive organ. We previously showed that the highly conserved Hippo signaling pathway regulates proliferation of both germ line and somatic cells in the *D. melanogaster* larval ovary. Response to Hippo signaling appeared to be mediated by different genetic mechanisms in germ line and soma, but the mechanism allowing distinct responses to the same signaling pathway remained unknown. Here we perform cell type-specific RNA-Seq of isolated germ line and somatic cells from the developing ovary at multiple time points spanning the formation of germ line stem cell niches, in either a Hippo signaling loss- or gain-of-function genetic background. Applying network analysis to these data revealed a novel regulator of ovarian development, the transcription factor *chinmo*. Subsequent experimental validation showed that *chinmo* acts as a key germ cell-specific translator of Hippo signaling in the developing ovary, allowing the Hippo signal to be transduced in cell type-specific ways in germ line and somatic cells within the same organ.

KEY WORDS: Yorkie, ovariole number, FACS, RNA-Seq, Larva, Ovary, *Drosophila*

INTRODUCTION

Animal organs are not heterogeneous masses of cells. Instead, they are composed of multiple cell types that contribute to the same organ, but have distinct gene expression profiles, morphologies, behaviours, and functions. In most organ systems, all these distinct cell types are somatic cells derived from the same germ layer (Barresi and Gilbert 2023). An important exception to this rule is found in the gonads (ovaries and testes), which contain both somatic cells of mesodermal origin, and cells of the germ line, destined to make eggs and sperm (Extavour 2007). Gonads are typically assembled after the specification of germ layers and of the germ line, but before gametogenesis begins. During gonadogenesis, somatic and germ cells proliferate, exchange neighbors, change their shapes and gene expression profiles, and create the final functional anatomical organization of the gonad. As for other systems of organogenesis, cell-cell signaling is crucial for this process. However, each unique cell type within the developing organ often has a distinct, cell type-appropriate response to the same incoming signals, allowing correct organ formation and function. Here we use the *Drosophila melanogaster* (fruit fly) ovary as a study system to elucidate how different cell types within the same organ can differently transduce the same signaling inputs during development.

A single adult ovary in *D. melanogaster* is made up of an estimated 26 distinct cell types (Rust et al. 2020) that are assembled into 16-23 tubular egg producing subunits called ovarioles (Büning 1994), making it an excellent model to study the regulation of organ size and subunit number (Sarikaya and Extavour 2015; Kumar et al. 2020). Ovariole number varies by up to four orders of magnitude across insect species, and in some insects, including Drosophilids, it is positively correlated with egg-laying and therefore fitness (Church et al. 2021; David 1970). In *Drosophila* species, ovariole number is established in the larval stages and determined by the number of stacks (called terminal filaments: TFs) of a specific type of somatic cell (terminal filament cells: TFCs) (King 1968,Honěk 1993,Markow 2007,Hodin 2009,Green 2012,Sarikaya

60 2019). The number of these stacks of cells, in turn, is determined by the number and stacking
61 dynamics of the component TFCs. We previously showed that TFC proliferation, and therefore
62 ovariole number, is regulated by the Hippo (Hpo) signaling pathway, which affects both TFC and
63 germ cell numbers (Sarikaya and Extavour 2015).

64 First discovered as a network of tumor overgrowth factors in *D. melanogaster* (Tapon et
65 al. 2002; Dong et al. 2007; Xu et al. 1995; Wu et al. 2003), the Hpo signaling pathway regulates
66 organ size, growth, cell proliferation and cell fate determination in animals. In the developing fruit
67 fly ovary, this pathway can regulate proliferation both cell-autonomously (based on cell-intrinsic
68 Hpo signaling activity) and non-cell autonomously (activity in one cell can affect proliferation in a
69 different cell) (Sarikaya and Extavour 2015). Regulation of cell proliferation in both the soma and
70 the germ line is essential for the normal development of the ovary, including species-specific
71 ovariole number. Members of the Hippo signaling pathway are expressed ubiquitously across
72 multiple distinct ovarian cell types that nevertheless have different proliferation dynamics
73 (Sarikaya and Extavour 2015). This begs the question of how differential regulation of Hpo
74 signaling may be achieved despite the potential for ubiquitous activation.

75 The canonical Hippo signaling pathway functions through regulating shuttling of the
76 transcriptional activator Yorkie (Yki) in and out of the nucleus. This shuttling is regulated by the
77 function of the serine-threonine kinase Hpo in conjunction with a cascade of kinases that ends
78 with the phosphorylation of Yki, preventing its nuclear localisation (Oh and Irvine 2008; Huang et
79 al. 2005). Under this model, unphosphorylated Yki enters the nucleus to form tissue-specific
80 transcriptional regulatory complexes (Slattery et al. 2013) with loading proteins like Scalloped (Sd)
81 and Homothorax (Hth). These transcription cofactor complexes bind to DNA and activate a wide
82 range of target genes, including many necessary for growth and proliferation (Wu et al. 2008;
83 Zhang et al. 2008; Zhao et al. 2008). Phosphorylation of Yki by other kinases, including Nemo-
84 like kinase and AMP-activated protein kinase, can either prevent or enhance Yki's targeting by

85 the canonical Hpo kinases, allowing a Hpo-independent mode of Yki regulation (Moon et al. 2017;
86 Wang et al. 2015). Furthermore, changes in the binding dynamics of Sd, the coactivator of Yki,
87 adds another layer of Yki regulation (Manning et al. 2024). Lastly, mechanical stress and proximity
88 of cell membranes during cell growth and proliferation can also regulate the Hpo signaling activity
89 (Zhao et al. 2007). Across animals, the Hpo pathway regulates multiple cellular processes *via* Yki
90 target genes, including cell size, cell proliferation, adhesion and apoptosis (Zheng and Pan 2019),
91 while interacting with other signaling pathways such as JAK-STAT, Notch, Hedgehog and EGFR
92 (Besse 2005,Matsuoka 2013,Sarikaya 2015,Yatsenko 2021,Song 2007,Kumar 2020) .

93 Previously, we showed that Hpo pathway activity regulates cell proliferation in multiple *D.*
94 *melanogaster* ovarian cell types, which in turn can determine the numbers of TFCs, TFs and
95 ultimately ovarioles (Sarikaya and Extavour 2015). RNAi-mediated knockdown of *hpo* or *wts* in
96 somatic cells increased TF and TFC number, while RNAi against *yki* decreased the numbers of
97 both cell types (Sarikaya and Extavour 2015). In this context, we demonstrated that the Hpo
98 pathway interacts with the EGFR pathway to regulate numbers of another somatic cell type, called
99 intermingled cells (Sarikaya and Extavour 2015) and with JAK-STAT signaling to regulate TFC
100 proliferation and the homeostasis between intermingled cells and germ cells (Sarikaya and
101 Extavour 2015). Furthermore, our RNAi screen in a *hpo* knockdown background in the larval ovary
102 identified a gene interaction network implicating all known conserved animal signaling pathways
103 in regulating *D. melanogaster* ovary development and function, including establishment of correct
104 ovariole number (Kumar et al. 2020).

105 To our surprise, our previous study showed that in contrast to somatic cells, *hpo*
106 knockdown did not affect germ cell number (Sarikaya and Extavour 2015). However, *yki*
107 knockdown reduced germ cell number significantly, as it did in somatic cells. This result suggested
108 the existence of a Hpo-independent mechanism of Yki activity in the germ cells (Sarikaya and
109 Extavour 2015). However, a mechanistic explanation for the differential response of germ cells

110 and somatic cells to these Hpo signaling components remains lacking. Given the variation in
111 outcomes of Hpo pathway abrogation in the germ cells and the somatic cells, we sought to use
112 cell type-specific transcriptional profiling to identify distinct gene regulatory responses to *hpo* or
113 *yki* activity in soma versus germ line. Here we present the results of this approach, wherein we
114 analyze stage- and tissue-specific transcriptomic datasets generated in three distinct genetic
115 backgrounds to assess the role of Hpo signaling and its interacting pathways in the cell types of
116 the developing *D. melanogaster* larval ovary. We reveal the transcription factor Chinmo as a
117 putative novel regulator of germ cell-specific Hpo-dependent activity and provide experimental
118 validation of this regulatory interaction in the developing ovary. Further, we provide evidence that
119 *chinmo* regulates the previously observed (Sarikaya and Extavour 2015) non-autonomous effect
120 that Hpo activity in germ cells exerts on neighboring somatic cells. Thus, our results show how
121 variation in the expression of cell type-specific targets can produce distinct proliferation response
122 outcomes to the same signaling inputs within a developing tissue.

123

124 **RESULTS**

125

126 ***hpo* and *yki* knockdown in somatic and germ line tissues**

127 *D. melanogaster* ovaries are made up of subunits called ovarioles (Figure 1A), whose number is
128 established at the third larval instar stage, 72-120 hours after egg laying (hAEL) at 25ºC (Figure
129 1B) (King 1970). The number of ovarioles in the adult directly corresponds to the number of TFs
130 formed in the larval ovary (Figure 1B), because TFs are neither formed nor destroyed during the
131 pupal phase that separates larva from adult (King 1970). The Hpo signaling pathway regulates
132 TF number by determining the number of TFCs available to assemble into TFs (Sarikaya and
133 Extavour 2015). We reasoned that the genetic mechanisms of Hpo regulation of TF number might

134 be revealed by determining the responses of germ cells and somatic cells to Hpo signaling activity
135 during TF formation (Sarikaya and Extavour 2015). We therefore selected larvae over three
136 stages of early ovary morphogenesis as follows: (1) before TF formation (Early = 72 hAEL; Figure
137 1Bi); (2) during TF formation (Middle (mid) = 96 hAEL; Figure 1Bii); and (3) after TF formation
138 (Late = 120 hAEL; Figure 1 Biii). We expressed GFP specifically in either the somatic cells (red
139 cells in Figure 1C) or in the germ cells (blue cells in Figure 1C) using cell type-specific GAL4
140 drivers (Brand and Perrimon 1993) (see Methods) and isolated somatic and germ cells
141 respectively using Fluorescence-Activated Cell Sorting (FACS) (Supplemental Figure S1). We
142 had previously established the gene expression profiles of wild type somatic and germ cells at
143 these stages (Tarikere et al. 2021). In the present study, we used the UAS/GAL4 system (Brand
144 and Perrimon 1993) to knock down either *hpo* or *yki* in either somatic or germ cells across the
145 three developmental stages described above, and then performed tissue-specific RNA-Seq to
146 identify the transcriptional regulatory effects of these two main components of the Hpo signaling
147 pathway on larval ovary development and morphogenesis (Figure 1D-E).

148

149 **The Hpo pathway regulates gene expression differently in the ovarian germ line and soma**
150 Our RNA-Seq study produced 48 independent datasets (Supplemental Table S1) of gene
151 expression in germ cells and somatic cells in two different knockdown conditions and at three
152 developmental stages. To identify and understand the variation in gene expression across
153 samples, we performed a principal component analysis (PCA). Our results showed that 51.5% of
154 the variation across all datasets was explained by cell type (Figure 2A). The first principal
155 component clearly separated somatic cells from germ cells (PC1 in Figure 2A). Cell type-specific
156 gene expression included both genes with known roles in the germ line (e.g. *vasa* (Lasko and
157 Ashburner 1988) and *bruno* (Kim-Ha et al. 1995) or in the somatic gonad (e.g. *traffic jam* (Li et al.
158 2003) and *bab2* (Godt and Laski 1995), as well as novel genes without such roles previously

159 described (Supplemental Table S2). The second greatest impact on transcriptional variation
160 (PC2) was developmental stage (Figure 2A).

161 We then performed individual PCA analysis of somatic cells (Figure 2B) and germ cells
162 (Figure 2C), which allowed us to better observe the effects of the two RNAi knockdown conditions
163 on the sample clustering. In the somatic cells, most of the variation (32.3%) amongst the samples
164 was attributable to developmental stage rather than to genotype (stages are indicated as distinct
165 shapes along PC1 in Figure 2B). Along the PC2 axis, datasets were sorted by genotype, with
166 both the *hpo* and *yki* loss-of-function treatments segregating in opposite directions relative to the
167 control across all three developmental stages (colors along PC2 in Figure 2B). By contrast, in the
168 germ cells, the samples clustered by genotype rather than by stage (colors along PC1 in Figure
169 2C). The *hpo* and *yki* loss-of-function conditions clustered together independently of
170 developmental stage, but far from the respective controls (Figure 2C).

171 These results suggest that *yki* and *hpo* regulate transcriptional activity in ovarian germ
172 cells and somatic cells differently during larval development. In the soma, the two genes have
173 distinct and stage-specific impacts on the transcriptomic landscape. In contrast, loss of function
174 of both genes generates very similar effects on the transcriptomes of the germ line, and these
175 regulatory impacts do not change significantly across the period of development studied here. To
176 better understand this variation at the level of individual genes in each cell type sample, we
177 performed a differential gene expression (DGE) analysis of *hpo* and *yki* knockdown conditions
178 compared to the corresponding control samples at each stage. In general, we found more
179 differentially expressed genes in germ cells than in somatic cells, when either *hpo* or *yki* levels
180 were reduced (Figure 2D, Supplemental Table S3).

181 In the soma, there was a similar number of upregulated (365) and downregulated (310)
182 genes (17.7%) under *hpo* knockdown, compared to over 60% more upregulated (231) than
183 downregulated (143) genes (61.5%) under *yki* knockdown (Figure 2D, Supplemental Table S3).

184 In contrast, in the germ cells we observed on average over twice as many down-regulated genes
185 (1,161 and 1,120 under *hpo* and *yki* knockdown respectively) as upregulated genes (421 and 600
186 under *hpo* and *yki* RNAi respectively) in both knockdown conditions. Interestingly, this much larger
187 number of differentially expressed *hpo*- and *yki*-responsive genes in the germ line did not
188 correspond with a notable change of the germ line transcriptional landscape throughout the
189 developmental period under study (Figure 2C). The soma, on the other hand, exhibited distinct
190 gene expression responses to Hpo signaling over developmental time (Figure 2B), and these
191 differential responses were explained by a comparatively small number of genes (Figure 2D). We
192 had previously observed that in the somatic cells, the cell proliferation phenotypes induced by the
193 reduction of *hpo* and *yki* activity were diametrically opposed (Sarikaya and Extavour 2015).
194 Consistently, differential gene expression analysis of *hpo* and *yki* knockdown conditions showed
195 that in the soma, most of the differentially regulated genes (75%) were exclusive to each genotype
196 (*hpo RNAi* 55% and *yki* RNAi 20%) (Figure 2E). Of all the differentially expressed genes, the
197 expression of only four genes (*apterous*, *CG11400*, *wrapper*, and *expansion*) was significantly
198 affected in opposite ways by *hpo* and *yki* RNAi treatment (Figure 2E). By contrast, in the germ
199 cells the majority (51%) of the differentially expressed genes were common to both *hpo* and *yki*
200 loss of function conditions (869 commonly downregulated and 245 commonly upregulated), and
201 only one gene (*CG34408*) showed an “opposite” expression change (upregulated in *yki* loss of
202 function and downregulated in *hpo* loss of function) (Figure 2F). These results are consistent with
203 the above-described observations that *yki* and *hpo* knockdowns induced similar changes in the
204 germ line transcriptome (Figure 2C), but induced genotype-specific effects on the transcriptome
205 of the soma (Figure 2B).

206

207 **Functional prediction analysis of the differentially expressed genes**

208 The differentially expressed genes in the germ cells included more significantly enriched
209 pathways from the Kyoto Encyclopedia of Genes and Genomes (KEGG) and terms from the Gene
210 Ontology (GO) database than the genes differentially expressed in the soma (Figure 3,
211 Supplemental Figure S2). We found that the Hippo, MAPK, Hedgehog, and TGFβ pathways were
212 significantly enriched among the downregulated genes in the germ line under both *hpo* and *yki*
213 knockdown conditions (Figure 3). We additionally found that DNA replication and mismatch repair
214 pathways were enriched within the genes upregulated in response to *hpo* knockdown in germ
215 cells. In the germ line response to *yki* knockdown, we observed enriched GO terms relevant to
216 meiosis and cell cycle regulation (Supplemental Figure S2a). In contrast, somatic ovarian cells
217 displayed very few significantly altered pathways under either knockdown condition (Figure 3).
218 GO analysis revealed that members of some of the same processes that were downregulated in
219 the germ line, were downregulated in somatic *hpo* knockdowns, but with fewer gene counts than
220 those in germ cells (Supplemental Figure S2). These processes included cell adhesion, taxis,
221 motility, tissue growth, cell proliferation, stem cell population maintenance, maintenance of cell
222 number, cell proliferation and cell death.

223

224 ***yki* is downregulated under *hpo* knockdown in the germ line but not the soma**

225 Our previous work suggested that Yki functions downstream of Hpo in the soma but independently
226 of Hpo in the germ line (Sarikaya and Extavour 2015). We used our cell-type-specific
227 transcriptomes to determine whether this functional difference was reflected at the level of
228 transcript regulation in one or both of germ line and soma. As expected, we observed a significant
229 reduction (adjusted p-value<0.05) of *hpo* transcript levels across all stages and in both cell types
230 under *hpo* knockdown (Figure 4A). The levels of *yki* transcript were also down-regulated (adjusted
231 p-value<0.05) by *yki* RNAi in all stages and in both cell types, with two apparent exceptions

232 (Figure 4B). First, we noted that the 1.4-fold downregulation of *yki* under *yki* RNAi in early-stage
233 somatic cells just missed our significance threshold (adjusted p-value 0.055). Furthermore,
234 somatic cells at this stage displayed a different transcriptional landscape than controls, consistent
235 with *yki* knockdown (Figure 2B). Second, we noted that one of the control samples for mid stage
236 germ cells had anomalously low levels of *yki* transcript compared to other control samples of the
237 same and other stages (outlined in red in Figure 4B). Removal of this putative outlier revealed a
238 significant reduction of *yki* under yki RNAi (Supplemental Figure S3). Thus, we conclude that both
239 RNAi conditions were able to significantly reduce the transcript levels of their respective target
240 genes, and that our analytical methods were able to detect this reduction.

241 In terms of the effect of RNAi against these two genes on the transcript levels of the other,
242 we found that *yki* transcript levels were significantly reduced under *hpo* RNAi in late stage germ
243 cells, but not at earlier stages, and not in any stage in the soma (Figure 4B).*yki* RNAi (log2FC=-
244 1) and the *hpo* RNAi (log2FC=-0.8) conditions caused a similar reduction in *yki* transcript in the
245 germ line at this late stage. In contrast, the knockdown of *yki* did not yield a significant change in
246 *hpo* transcript levels in either cell type at any stage (Figure 4A). A possible exception may be the
247 mid stage germ cells: when the control sample with anomalously low levels of *yki* is excluded,
248 *hpo* appears significantly downregulated under *yki* knockdown with a fold change of -1.1
249 (Supplemental Figure S3). The degree of possible down-regulation of *hpo* in the *yki* RNAi
250 condition is much weaker (Log2FC=-1.1) than the reduction of *hpo* produced by the *hpo* RNAi
251 condition at the same stage (Log2FC=-4.1) (Figure 4A). Taken together, our results suggest that
252 the transcriptional regulatory relationship between *hpo* and *yki* in the larval female germ line is
253 complex, different from that in the soma, developmental stage-specific, and not directly predicted
254 from previous observations on the regulatory interactions of their protein products.

255

256 **Gene regulatory network analysis suggests *chinmo* as a novel mediator of *hpo*-dependent**
257 ***yki* regulation**

258 To generate hypotheses as to how *hpo* might regulate *yki* expression in the larval germ line, we
259 performed a network analysis. To this end, we built a directed network using the DroID database
260 of protein-protein interactions and transcription factor-encoding genes (Murali et al. 2011; Yu et
261 al. 2008). Additionally, we used publicly available Yki and GAF Chip-seq data from *D.*
262 *melanogaster* embryo, wing disc and S2 cells (Oh et al. 2013) to find possible direct targets of Yki
263 in *D. melanogaster* and added them into the network. From the ChIP-seq Yki data, we identified
264 1,513 peaks of Yki-binding regions, which we mapped to the closest gene, thus identifying 1,118
265 genes putatively regulated by Yki across the three studied cell types. By taking the intersection of
266 sets of putative Yki targets from all three cell types, we hoped to retrieve targets of Yki that might
267 also be relevant in the ovary.

268 In the germ line, 31.4% and 33.4% respectively of all the genes downregulated in either
269 *hpo* or *yki* knockdowns were putative direct targets of Yki (Supplemental Figure S4). Conversely,
270 of the 1,118 putative Yki targets in our network that were differentially expressed, most of them
271 were downregulated (94.59% under *hpo* RNAi and 79.14% under *yki* RNAi) (Supplemental Figure
272 S4). In contrast, in somatic cells only 8.23% and 2.86% of putative Yki target genes were
273 significantly affected by *hpo* and *yki* knockdowns respectively (Supplemental Figure S4).
274 Similarly, among the differentially expressed putative Yki targets the downregulated fraction was
275 much lower in the somatic cells than observed in the germ cells (67.37% were downregulated
276 under *hpo* knockdown, and 50% under *yki* knockdown; Supplemental Figure S4). This is
277 consistent with the overall much higher number of differentially regulated *hpo*- and *yki*-responsive
278 genes in the germ cells relative to somatic cells (Figure 2D)

279 We found that the shortest path linking *hpo* and *yki* in the network was through a predicted
280 interaction of Hpo with a transcription factor called Chronologically inappropriate morphogenesis

281 (Chinmo), which was predicted to regulate *yki* expression (Figure 4C). Moreover, Chinmo was the
282 sole candidate in our interaction network that was predicted to directly link both Hpo and Yki
283 (Figure 4C). Our RNA-Seq data showed that this transcription factor is significantly upregulated
284 in late stage germ cells under both *hpo* and *yki* loss of function conditions, and conversely, was
285 significantly downregulated in late stage somatic cells under both RNAi conditions (Supplemental
286 Figure S5). We therefore considered the hypothesis that differential *chinmo* expression and/or
287 function between germ line and soma might contribute to the different responses of those cell
288 types to Hpo pathway activity and sought to test this hypothesis experimentally.

289

290 **Nuclear Chinmo in the Germ cells is regulated by *yki* expression**

291 Our RNA-Seq results indicated that *chinmo* is expressed at constant levels in wild type germ line
292 cells throughout the developmental stages studied here, while levels of *chinmo* decreased over
293 developmental time in the ovarian somatic cells (Supplemental Figure S5). Given that *chinmo*
294 encodes a transcription factor (Zhu et al. 2006; Chen et al. 2020), we used an anti-Chinmo
295 antibody to examine the expression of Chinmo protein in the cells of the larval ovary. We detected
296 high levels of Chinmo protein in the nuclei of the germ cells in mid and late stages of larval
297 development, but only weak expression in the somatic ovarian cells (Figure 5A).

298 To determine the functional significance of *chinmo* expression in the larval ovary, we
299 reduced *chinmo* expression in either the somatic cells or the germ line cells. We used ovariole
300 number as a measure of effective change in phenotype in comparison with the *RNAi* knockdowns
301 of our predicted interactors of Chinmo in this context, Hpo and Yki, both of which we previously
302 identified as regulating ovariole number (Sarikaya and Extavour 2015). We found that, consistent
303 with the weakly detected Chinmo protein in the soma, reduction of *chinmo* in the somatic cells,
304 unlike the reduction of either *hpo* or *yki,* caused no significant change in ovariole number (Figure
305 5B; Supplemental Table S4). In contrast, abrogation of *chinmo* in the germ cells caused a

306 significant increase in ovariole number, as did reduction of *hpo* in the germ cells (Figure 5B;
307 Supplemental Table S4). Reducing levels of y*ki* in the germ cells did not cause any change in
308 ovariole number (Figure 5B; Supplemental Table S4).

309 Our network model predicted a putative transcriptional regulatory relationship between *yki*
310 and *chinmo*, and a potential protein-protein interaction between Hpo and Chinmo proteins. We
311 therefore asked whether levels of *yki* or *hpo* gene activity influenced the levels of Chinmo protein
312 in the developing ovary. Consistent with our network model, Chinmo protein levels were not
313 significantly affected by *hpo RNAi* (Figure 5C). Similarly, reduction of *chinmo* or *yki* expression in
314 somatic cells did not significantly alter detectable Chinmo protein levels in germ cells (Figure 5C;
315 Supplemental Table S4). However, Chinmo protein levels did significantly increase in the germ
316 cells upon *hpo* knockdown in somatic cells (Figure 5C; Supplemental Table S4), indicating a non-
317 cell autonomous role for Hpo in Chinmo regulation in the germ line. Reduction of *chinmo* or *yki* in
318 the germ line caused a reduction in detectable Chinmo protein in these cells (Figure 5C;
319 Supplemental Table S4).

320 To understand the functional outcomes in the ovary of Chinmo levels in the larval germ
321 cells (Figure 5C; Supplemental Table S4), we quantified germ cells, TFCs, and TFs at the late
322 larval stage, and ovarioles in the adult, under loss of germ line expression of *chinmo*, *yki* and *hpo*.
323 Reduction of *chinmo*, but not *yki* or *hpo*, in the germ cells led to a significant increase in germ cell
324 number when compared to both *GAL4* or *[RNAi]* controls (Figure 5D; Supplemental Table
325 S4). We found that the increase in ovariole number caused by reduction of *chinmo* or *hpo* in the
326 germ cells (Figure 5B; Supplemental Table S4) was the result of a non-cell-autonomous increase
327 in TFC number and in TF number (Figure 5E; Supplemental Table S4). Interestingly, reduction in
328 *chinmo* levels in the germ line also caused an increase in the number of TFCs in each TF (Figure
329 5E; Supplemental Table S4). Consistent with the observation that *yki* reduction in germ cells did

330 not change ovariole number (Figure 5B; Supplemental Table S4), this genetic background also
331 had wild type numbers of TFCs and TFs (Figure 5E; Supplemental Table S4).

332 Taken together, these data are consistent with the hypothesis that Chinmo protein in the
333 nucleus of germ cells regulates germ cell number cell-autonomously, and that Chinmo protein
334 levels in the germ line require germ line expression of *yki*. Further, expression of *chinmo* and
335 *hippo* in the germ cells also exerts a non-cell autonomous effect on somatic cells, limiting TFC
336 number, TF number, and hence ovariole number.

337

338 **DISCUSSION**

339 We have provided evidence for a novel genetic mechanistic hypothesis to explain the differential
340 response of germ line and somatic cells to the Hpo signaling pathway during the larval
341 development of the *D. melanogaster* ovary. We propose that the transcription factor Chinmo acts
342 as a modifier of Hpo-independent cell number regulation of the germ line, but not of the somatic
343 gonad cells.

344

345 **The Hippo pathway has distinct effects on transcription in the germ cells and the soma of**
346 **the larval ovary**

347 In this study, we knocked down either *hpo* or *yki* using RNAi driven in either the germ cells or the
348 somatic cells, thus providing us with a lens into the effects of each of these genetic manipulations
349 on the transcriptomic landscapes in each cell type. The canonical understanding of the Hippo
350 signaling pathway suggests that the presence of phosphorylated Hpo in the cellular milieu
351 prevents the nuclear localization of Yki and therefore the downstream expression of its target
352 genes. Under this model, the absence of Hpo in the cytoplasm allows Yki to remain

353 unphosphorylated, enter the nucleus, and drive the expression of its downstream targets. This
354 model therefore predicts a different transcriptional profile with and without Hpo. Our observation
355 that knockdown of either *hpo* or *yki* in the soma impacted transcript levels of two mutually
356 exclusive sets of genes supports the canonical understanding of the Hippo signaling pathway
357 (Figure 2B). In the germ cells, however, this is not the case: the effects of the knockdown of either
358 *hpo* or *yki* caused transcriptional changes in a similar set of genes (Figure 2C). This suggests that
359 *hpo* and *yki* RNAi have different effects on the transcriptome of the soma, but similar effects on
360 germ line.

361 Furthermore, we found that more genes were differentially expressed in the germ line than
362 in the soma (Figure 2D). The higher number of differentially expressed *yki*-regulated genes in
363 somatic tissues could mean that *yki* directly or indirectly represses more genes in somatic tissue
364 than it activates. Again, we observed differences in the effect of *hpo* and *yki* knockdown on germ
365 cells and somatic cells. The higher number of downregulated genes in the germ cells under these
366 conditions suggests that *hpo* and *yki* may operate in germ line tissue primarily through promoting
367 the transcription of genes rather than repressing them. In all genetic backgrounds, we observed
368 that most of the transcriptional variation in the soma was attributable to the progression of
369 development (Figure 2B), while in the germ line, the greatest variation between the samples was
370 due to abrogation of Hippo signaling pathway function (Figure 2C). This suggests that many of
371 the transcriptome differences we observed in the soma across development reflect the dynamic
372 morphogenetic changes taking place in the somatic cells of the ovary during the process of
373 terminal filament determination and organization.

374

375 ***Hpo* RNAi in germ cells does not affect cell number via *yki* repression**

376 The similar transcriptomic impact of *yki* and *hpo* knockdowns in the germ cells is intriguing given
377 their opposite phenotypic effects on cell proliferation in the soma (Sarikaya and Extavour 2015).
378 We had previously shown that *hpo* knockdown in somatic cells increased their number, while *yki*
379 knockdown decreased their number (Sarikaya and Extavour 2015). Similarly, overexpression of
380 *hpo* and *yki* in somatic cells and in germ cells also had opposite phenotypic effects, whereby *hpo*
381 overexpression reduced somatic cell number and *yki* knockdown increased it (Sarikaya and
382 Extavour 2015). These results were consistent with the canonical model of Hippo pathway activity.
383 However, although *yki* knockdown in germ cells decreased germ cell number, *hpo* knockdown did
384 not change it. We suggest that transcriptional regulation of *yki* by *hpo* may contribute to the
385 previously reported apparent imperviousness of germ cell number to *hpo* knockdown. We noted
386 that in the germ line, a reduction in *hpo* caused a reduction in *yki* (Figure 4B), but that there was
387 no detectable regulation of *hpo* by *yki* (Figure 4A). To our knowledge, this is the first reported
388 example of the transcriptional regulation of *yki* by *hpo.* We hypothesize that when *hpo* is reduced
389 in germ cells, although nuclear localization of Yki is not inhibited, there is less *yki* transcript. This
390 could in principle lead to less Yki protein and less efficient triggering of the transcriptional cascade
391 that would result in a cell number increase. In sum, we hypothesize that a balance of *hpo* and *yki*
392 transcript levels contributes to regulating the number of germ cells.

393

394 ***Chinmo* and its role in the regulation of *hpo* and *yki***

395 The transcription factor *chinmo* is the only gene we found in our network analysis predicted to
396 directly regulate *yki* in response to *hpo* levels, since Hpo and Chinmo proteins have the potential
397 to interact based on yeast two hybrid data (Yu et al. 2008). Furthermore, our network predicts that
398 *chinmo* has the potential to regulate the expression of both *hpo* and *yki*, and that in turn, *yki* could
399 regulate the expression of Chinmo based on ChIP-seq data (Oh et al. 2013). We hypothesize that
400 *chinmo* could be involved in regulating *yki* transcript levels in response to Hpo activity levels,

401 which would provide a mode of control of Hpo by Yki through Chinmo. Previous studies of *chinmo*
402 in the *D. melanogaster* testis and ovaries showed that it plays a key role in inducing male fate in
403 somatic cells of the testis, but that it is not required in ovarian somatic cells (Ma et al. 2016).
404 Consistent with that report, our results show increased expression of *chinmo* in response to *yki*
405 knockdown in the germ line but not in the soma (Supplemental Figure S5).

406 Chinmo is a BTB-Zinc finger transcription factor that is conserved across insects (Spokony
407 and Restifo 2007; Nadimpalli et al. 2015). Chinmo was first identified as a negative regulator of
408 the JAK/STAT signalling pathway (Flaherty et al. 2009; Fisher et al. 2012; Wang et al. 2013) and
409 acts as a transcriptional repressor downregulating the expression of a broad spectrum of genes
410 including *shotgun* (*E-Cadherin*) (Enomoto et al. 2021), *β Spectrin*, *polychaetoid*, *scribble* and
411 *mirror* (Grmai et al. 2021). In some studied contexts, Chinmo prevents the differentiation of cells
412 and promotes their ability to proliferate (Chafino et al. 2023) .

413 Given the low levels of detectable Chinmo in somatic nuclei of the larval ovary (Figure
414 5A), and that adult ovariole number is unchanged by somatic reduction of *chinmo* (Figure 5C), we
415 hypothesize that Chinmo does not act in somatic cells to impact the known regulation of the
416 number of TFCs, TFs or ovarioles by *hpo* or *yki* (Sarikaya and Extavour 2015). In contrast, we
417 detected Chinmo protein in larval germ cell nuclei (Figure 5A), where its expression appears to
418 be dependent on *yki* levels in the germ cells (Figure 5C). Further, we observed that reduction of
419 *chinmo* in germ cells caused an increase in germ cell number (Figure 5D), suggesting that Chinmo
420 acts in larval ovarian germ cells to limit their proliferation. This is reminiscent of the observation
421 that in $chinmo^{ST}$ loss of function mutants, adult male germ cells overproliferate (Ma 2014) . On
422 the other hand, $chinmo^{-/-}$ clones in a heterozygous $chinmo^{+/-}$ background do not (Tseng 2021) .
423 Thus, the cell-autonomous impact of *chinmo* function on germ cell proliferation appears to be
424 context- and sex-specific. Combining the results presented herein with our previous

425 understanding of Hippo signaling in the ovary, we propose a model for the cell type-specific
426 regulation of *hpo*-mediated proliferation during larval ovary development (Figure 6).

427 In this model, Chinmo and Yki function in opposition to each other in the germ line to
428 regulate germ cell number, limiting or promoting germ cell proliferation respectively. Thus, unlike
429 in the somatic cells, loss of *hpo* in germ cells does not cause an increase in germ cell number
430 because Chinmo continues to prevent Yki-dependent transcription. The similarities that we
431 observed between the transcriptional profiles of the *hpo* and *yki* knockdown in the germ cells
432 might be explained by the prediction that Chinmo prevents Yki-dependent transcription in these
433 cells. Thus, we propose that the interplay of Chinmo and Yki levels in the nucleus contributes to
434 the maintenance of germ cell number, and that disrupting this balance causes a change in germ
435 cell number. This model is also consistent with the Hpo-independent function of Yki in the germ
436 cells that was suggested by our previous work (Sarikaya and Extavour 2015).

437

438 **Cell-non-autonomous effects of Chinmo and Hippo**

439 Reduction of somatic *hpo* causes a non-autonomous increase in the levels of detectable nuclear
440 Chinmo in the germ cells (Figure 5C). This could be due to *hpo* downregulation in either or both
441 of TFCs or intermingled cells, given that the GAL4 driver we used here (*tj:Gal4*) is expressed in
442 both somatic cell types (Sarikaya and Extavour 2015). We note that downregulation of *hpo* in
443 intermingled cells causes JAK/STAT pathway upregulation in germ cells (Sarikaya and Extavour
444 2015), and that Chinmo is positively regulated by the JAK/STAT signalling pathway (Flaherty et
445 al. 2009; Fisher et al. 2012; Wang et al. 2013). It is thus possible that abrogating *hpo* activity in
446 intermingled cells causes nuclear Chinmo levels to rise in the germ line because of the non-
447 autonomous upregulation of JAK/STAT activity in germ cells.

448 Our observation of the non-autonomous impact of germ cell number on multiple aspects
449 of TFC number and organization (Figure 5B, 5E) is a new and intriguing finding. Reducing *chinmo*
450 or *hpo* in the germ line led to a significant increase in TFC, TF (Figure 5E) and ovariole number
451 (Figure 5B), suggesting that germ cell number can positively regulate ovariole number, a
452 hypothesis that has remained underexplored in the field. In our previous work (Sarikaya and
453 Extavour 2015) we did not observe a statistically significant increase in germ cells in
454 *nos:GAL4>hpo*^{RNAi} larval ovaries (Sarikaya and Extavour 2015), which is the same genetic
455 background we used in the present work. Further, although we did not count ovarioles in our
456 previous analysis of the *nos:GAL4>hpo*^{RNAi} condition, we did not observe a statistically significant
457 non-autonomous impact of *hpo* knockdown in the germ line on terminal filament cell number. We
458 attribute these differences to the fact that the control genotypes used for comparison and
459 calculation of statistical significance in the present work (GAL4 or UAS heterozygotes obtained
460 by crossing the parent strains to wild type strain Oregon R), were slightly different from the control
461 genotypes used in our previous study (sibling controls) (Sarikaya 2015) . We and others have
462 observed that ovariole number, and its contributing developmental processes, are such highly
463 polygenic traits that even small changes in genetic background can have statistically detectable
464 effects (Coyne 1991,Thomas-Orillard 1976,Bergland 2008,Orgogozo 2006,Telonis-Scott
465 2005,WAYNE 2001,Wayne 2002,Kumar 2020) .

466 Although increasing ovariole number by increasing germ cell number has not, to our
467 knowledge, previously been reported, there are at least two reported examples of the inverse
468 situation, where reduced ovariole number is correlated with reduced germ cell number. In one
469 example, ovaries of adult females carrying the dominant female sterile *ovo*^{D1} allele, which lacks
470 functional adult female germ cells, have fewer ovarioles than wild type (Extavour 2000). This could
471 in principle be because of a reduction in total germ cell number during larval stages in this
472 genotype, which is consistent with the interpretation of larval germ line clonal analysis of this allele

473 (Perrimon 1984). In a second example, agametic adult females generated by irradiating the
474 posterior pole of embryos (Geigy 1931), have fewer ovarioles than controls (Aboïm 1945).

475 Finally, we note that reduction in *chinmo* levels in the germ cells also caused an
476 unexpected increase in the number of TFCs in each TF (Figure 5E). To our knowledge, this is the
477 first reported evidence of changes in germ line gene influencing TCF number and TF
478 morphogenesis. Determining the non-autonomous regulatory mechanism that allows larval germ
479 cells to impact the future fecundity of the adult, by influencing somatic morphogenesis of the
480 ovary, is an interesting avenue for future research.

481

482 **MATERIALS AND METHODS**

483

484 **Fly stocks**

485 Flies were reared as previously described (Sarikaya et al. 2012) at 25ºC and 60% humidity on
486 standard *Drosophila* food with yeast in uncrowded vials. The "wild type" genetic background
487 referred to herein is Oregon R (Lindsley and Grell 1968). The following fly lines were obtained
488 from the Bloomington *Drosophila* Stock Center (BDSC): *w[*]; P{w[+mW.hs]=GawB}bab1[Pgal4-*
489 *2]/TM6B, Tb[1]* (abbreviated herein as *bab:GAL4*; BDSC stock number 6803); *P{w[+mC]=UAS-*
490 *Dcr-2.D}1, w[1118]; P{w[+mC]=GAL4-nos.NGT}40* (abbreviated herein as *nos:GAL4*; BDSC
491 stock number 25751); *y w; P{w[+mW.hs]=GawB}NP1624* was obtained from the Kyoto Stock
492 Centre (abbreviated herein as *tj:*GAL4; stock number K104–055); *y[1] v [1];*
493 *P(y[+t7.7]v[+t1.8]=TRiP. HMS00006) attP2* (abbreviated herein as *hpo[RNAi]*; BDSC stock
494 number 33614) and *y[1] v[1]; P(y[+t7.7] v[+t1.8]=TRiP.HMS00041)attP2* (abbreviated herein as
495 *yki[RNAi]*; BDSC stock number 34067); *y[1] v[1]; P{y[+t7.7] v[+t1.8]=TRiP.JF02341}attP2*
496 (abbreviated herein as *chinmo[RNAi]*; BDSC stock number 26777). *w[1118], P[UAS Stinger]*

497 (abbreviated herein as *UAS:Green Stinger I*, (Barolo et al. 2000) used for GFP expression was
498 a gift from Dr. James Posakony (University of California, San Diego). Crosses (described below
499 in "Staging larvae") were set with 100-200 virgin females and 50-100 males in a 180 ml bottle
500 (with 50 ml media per bottle) one day prior to egg laying. For somatic *chinmo* knockdown via
501 RNAi, we used a *tj:GAL4* driver (Li et al. 2003), rather than the *bab*:*GAL4* driver (Cabrera et al.
502 2002), as the latter caused lethality when driving *chinmo [RNAi]* (data not shown).

503

504 **Staging larvae**

505 Uniformly staged larvae were collected from near-synchronously laid eggs. To obtain a desired
506 genotype, crosses were set as described above in "Fly Stocks" at 25°C at 60% humidity and left
507 overnight to mate. Hourly egg collections were set up on 60 mm apple juice-agar plates (9 g agar,
508 10 g sugar, 100 ml apple juice and 300 ml water) with a pea-sized spread of fresh yeast paste
509 (baker's yeast granules made into a paste with a drop of tap water). Eggs were collected hourly
510 for eight hours. The first two collection plates were discarded to remove asynchronously laid eggs
511 that may have been retained inside the females following fertilization. Staged first instar larvae
512 were collected into vials 24 hours after egg collection. Larvae at 72h hours After Egg Laying (h
513 AEL) were designated as early stage, at 96h AEL as middle stage and at 120h AEL as late stage
514 of terminal filament development.

515

516 **Dissection and dissociation of larval ovaries**

517 Staged larvae were collected for dissection every hour. Fat bodies were dissected out of the
518 larvae using a pair of forceps. Ovaries, located in the center of the length of each fat body, were
519 then dissected free of the fat body using an insulin syringe needle (BD 328418). Ovaries thus
520 dissected clear of fat body were collected in ice-cold DPBS (Thermo Fisher 14190144) and

521 batches of 20-30 ovaries in DPBS were kept on ice for a maximum of four hours until dissociation
522 and subsequent FACS processing. For dissociation, dissected ovaries in ice-cold DPBS were
523 transferred to 0.25% trypsin solution (Thermo Fisher 25200056) for ten minutes at room
524 temperature in the cavity of a glass spot plate (Fisher Scientific 13-748B). They were then
525 transferred to another cavity containing 2.5% liberase (5 g liberase reconstituted in 2 ml nuclease
526 free water; Sigma 5401119001), teased apart with tungsten needles until most of the clumps were
527 separated, and left in the liberase solution (without agitation) at room temperature for ten minutes.
528 The tissue in liberase was pipetted gently to uniformly mix and dissociate the cells. The cell
529 suspension was then transferred to an RNA Lobind tube (Eppendorf 8077-230) and placed on a
530 vortexer for 1 minute. This sample was immediately subjected to fluorescence activated cell
531 sorting (FACS) and the sorted cell suspension was collected in an RNA Lobind tube containing
532 100-200 µl Trizol (Thermo Fisher 15596026).

533

534 **Flow sorting GFP positive cells**

535 The dissociated cell suspension was sorted in a MoFlo Astrios EQ Cell sorter (Beckman Coulter)
536 run with Summit v6.3.1 software. The dissociated cell suspension was diluted and a flow rate of
537 200 events per second was maintained with < 98% sorting efficiency during the sorting process.
538 A scatter gate (R1) was employed to eliminate debris, and a doublet gate (R2) was used to
539 exclude non-singlet cells. A 488 nm emission Laser was used to excite the GFP, and the collection
540 was at 576 nm. The GFP-positive cells were designated in gate R3 and sorted directly into Trizol
541 (Supplemental Table S1). The resulting cells collected in Trizol were frozen immediately by
542 plunging the tube in liquid nitrogen and then stored at -80°C until RNA extraction. A single
543 replicate consisted of at least 1000 cell counts pooled from FACS runs.

544

545 **RNA extraction**

546 Flow sorted cells stored in Trizol at -80°C were thawed at room temperature and lysed with a
547 motorized pellet pestle (Kimble 749540-0000). A Zymo RNA Micro-Prep kit (Zymo Research
548 R2060) was used to isolate RNA from the homogenized Trizol preparations. An equal volume of
549 molecular grade ethanol (Sigma E7023) was added to Trizol and mixed well with a pellet pestle,
550 then pipetted onto a spin column. All centrifugation steps were done at 10,000g for one minute at
551 room temperature. The column was washed with 400 µl Zymo RNA wash buffer and then treated
552 with Zymo DNase (6 U/µl) for 15 minutes at room temperature. The column was then washed
553 twice with 400 µl Zymo RNA Pre-wash buffer and once with Zymo RNA wash-buffer. The RNA
554 was eluted from the column in 55 µl of nuclease-free water (Thermo Fisher 10977015). The RNA
555 obtained was quantified first using a NanoDrop (Model ND1000) spectrophotometer and then
556 using a high sensitivity kit (Thermo Fisher Q32852) on a Qubit 3.0 Fluorometer (Thermo Fisher
557 Q33216). The RNA was also checked for integrity on a high sensitivity tape (Agilent 5067-5579)
558 with an electronic ladder on an Agilent Tapestation 2200 or 4200.

559

560 **Library preparation**

561 cDNA libraries were prepared using the Takara Apollo library preparation kit (catalogue #
562 640096). Extracted RNA samples were checked for quality using Tapestation tapes. 50µl of RNA
563 samples were pipetted into Axygen PCR 8-strip tubes (Fisher Scientific 14-222-252) and
564 processed through PrepX protocols on the Apollo liquid handling system. mRNA was isolated
565 using PrepX PolyA-8 protocol (Takara 640098). The mRNA samples were then processed for
566 cDNA preparation using the PrepX mRNA-8 (Takara 640096) protocol. cDNA products were then
567 amplified for 15 cycles of PCR using longAmp Taq (NEB M0287S). During amplification PrepX
568 RNA-Seq index barcode primers were added to each library to enable multiplexing. The amplified
569 library was then cleaned up using PrepX PCR cleanup-8 protocol with magnetic beads (Aline C-

570 1003). The final cDNA libraries were quantified using a high sensitivity dsDNA kit (Thermo Fisher
571 Q32854) on a Qubit 3.0 Fluorometer (Thermo Fisher Q33216). cDNA content and quality were
572 assessed with D1000 (Agilent 5067-5582) or high sensitivity D1000 tape (Agilent 5067-5584, for
573 low quantities of cDNA) on an Agilent Tapestation 2200 or 4200.

574

575 **Sequencing cDNA libraries**

576 Libraries were sequenced on an Illumina HiSeq 2500 sequencer. Single-end 50bp reads were
577 sequenced on a high-throughput flow cell. Libraries of varying concentrations were normalized to
578 be equimolar, the concentrations of which ranged between 2-10nM per lane. All the samples in a
579 flow cell were multiplexed and later separated based on unique prepX indices to yield at least 10
580 million reads per library. The reads were demultiplexed and trimmed of adapters using the
581 bcl2fastq2 v2.2 pipeline to yield final fastq data files.

582 Three RNA-Seq biological replicates were obtained for each condition, each of which had
583 at least 10 million reads. The only exception was the early-stage germ line under both *hpo* and
584 *yki* RNAi knockdowns, for which we only obtained a single biological replicate due to the technical
585 challenge of obtaining enough germ line cells from these knockdown ovaries. These single
586 replicates of early germ line stages were not included in the differential expression analysis but
587 are made publicly available as part of the reported dataset (See Data Availability).

588

589 **Immunohistochemistry**

590 Larvae were dissected as previously described (Sarikaya et al. 2012; Sarikaya and Extavour
591 2015) and stained as previously described. For all cell counts, samples were dissected at the
592 larval-pupal transition stage. Primary antibodies and the concentrations used to stain the larval-
593 pupal transition stage ovaries are as follows: Mouse anti- Engrailed 4D9 (1:40, Developmental

594 Studies Hybridoma Bank (DSHB)), Rabbit anti-Vasa (1:3000, gift from A. Nakamura, Kumamoto
595 University), Rat anti-Chinmo (1:500, gift from E. Bach, New York University; (Wu 2012).
596 Secondary antibodies used were anti-mouse Alexa Fluor 488, anti-rat Alexa Fluor 488, and anti-
597 rabbit Alexa Fluor 568, all used at 1:400, and Hoechst 33342 used at 1:10,000 (stock solution 10
598 mg/mL). All samples were imaged on a Zeiss LSM 880 inverted laser confocal microscope. For
599 quantification of Chinmo expression levels, all samples were dissected and stained in parallel.
600 Imaging settings, including laser power, detector gain and step sizes, were kept constant for all
601 experimental and appropriate control samples.

602

603 **Quantification of ovariole number, cell number and Chinmo protein level**

604 Ovariole number was quantified as previously described (Kumar et al. 2020) . Germ cells were
605 counted manually in larval-pupal transition stage ovaries stained for Vasa protein, using the
606 Manual tracking with TrackMate plugin in Fiji (Schindelin et al. 2012; Tinevez et al. 2017) .
607 Terminal filaments and terminal filament cells in each terminal filament were counted manually in
608 larval-pupal transition stage ovaries stained for Engrailed, using the Cell counter plugin in Fiji.
609 Total terminal filament cell number per ovary was calculated by adding up the number of terminal
610 filament cells in each terminal filament.

611

612 **RNA-Seq data processing**

613 The *D. melanogaster* genome assembly and gene annotations were obtained from FlyBase
614 version dmel_r6.36_FB2020_05 (Larkin et al. 2020) . The reads were aligned with RSEM v1.3.3.
615 (Li and Dewey 2011) Using STAR v2.7.6a as read aligner, (Dobin et al. 2013) we obtained the
616 gene counts in each library. Because some of the tissue-specific biological samples were
617 sequenced in more than one lane or run, the reads were split into multiple fastq files, and the

618 gene counts belonging to the same biological sample were summed. Gene counts in each dataset
619 were normalized with the variance stabilizing transformation (VST) method implemented in the
620 DESeq2 v1.26.0 (Love et al. 2014) R package. Further analyses, such as principal component
621 analysis, hierarchical clustering, and differential expression analysis, were performed in R using
622 the VST-normalized counts.

623

624 **Differential expression analysis**

625 The differential expression analyses were performed with DESeq2 v1.26.0 (Love et al. 2014).
626 Genes with a Benjamini-Hochberg adjusted p-value lower than 0.05 were selected as differentially
627 expressed in the corresponding contrast.

628

629 **Functional predictions**

630 The Gene Ontology (GO) and Kyoto Encyclopedia of Genes and Genomes (KEGG) pathways
631 enrichment analyses were performed on the differentially expressed genes with the enrichGO
632 and enrichKEGG functions of the clusterProfiler package (v3.14.3) for R (Yu et al. 2012). The GO
633 terms were obtained using the R package AnnotationDbi (Carlson 2024) with the database
634 org.Dm.eg.db v3.10.0. The GO overrepresentation analysis of biological process was performed
635 against the gene universe of all *D. melanogaster* annotated genes in org.Dm.eg.db, adjusting the
636 p-values with the Benjamini-Hochberg method, adjusted p-value and q-value cutoff of 0.01, and
637 a minimum of 30 genes per term. For the KEGG enrichment analysis, p-values were adjusted by
638 the Benjamini-Hochberg procedure, and an adjusted p-value cutoff of 0.05 was used.

639

640 **Analysis of publicly available ChIP-Seq data**

641 We obtained the ChIP-Seq from GEO (GSE46305 and GSE38594) (Oh et al. 2013, 2014). We
642 downloaded the coordinates of the 3,749, 6,491, and 3,991 Yorkie-bound peaks from embryo
643 (E8-16h), wing imaginal discs, and S2 cells respectively. The coordinates of the peaks were
644 based on the *D. melanogaster* genome assembly BDGP release 5, and transformed to
645 coordinates for the latest genome version (release 6) with the lifterOver function. The peaks were
646 annotated with ChIPseeker (v.1.22.1) using *D. melanogaster* genome annotations from FlyBase
647 (v6.36). We defined the promoter region as the 1,500 bp flanking the transcription start site, and
648 69-75% of the peaks were found within the promoter regions of genes thus defined. In total 2,331,
649 3,931, and 2,247, genes with Yki-bound sites in the defined promoter region were identified, in
650 embryo, wing imaginal discs, and S2 cells respectively. 4,980 genes were unique (appeared only
651 in one dataset), 1,118 were common across the three datasets, and 2,406 were common to at
652 least two datasets. Following the same methodology, we analyzed the GAF (*Trl*) Chip-Seq peaks
653 (GSE38594) from embryo (E8-16h) and wing imaginal discs. Thus, we associated the 6,449 and
654 6,302 GAF-bound peaks from embryo and wing imaginal discs respectively to the promoters of
655 4,086 genes, of which 2,095 were common to both datasets.

656

657 **Network analysis**

658 We obtained the Transcription Factor – Gene (TF-gene) interaction network form the Drosophila
659 Interactions database (www.droidb.org, version DroId_v2018_08), containing 157,462
660 interactions of 12,323 genes. We added to this network the 1,118 interactions of Yorkie and the
661 2,095 interactions of GAF predicted from the ChIP-seq analysis. After removing redundancies,
662 we had 158,923 edges and 112,562 nodes in the network. We also obtained 127,353 unique
663 protein-protein interactions (PPI) between 10,632 proteins from DroID v2018_08. The TF-gene
664 and PPI networks were joined, yielding a network with 328,989 edges and 13,337 nodes while

665 designating as an edge attribute whether the interaction was a TF-gene or PPI. We assigned
666 directionality to the TF-gene edges because TFs regulate the target and not vice-versa while the
667 PPI edges were set as bi-directional. We looked for the shortest path in the network in which Hpo
668 could regulate Yki, and Chinmo emerged as the only possible connector, requiring only two steps.

669

670 **COMPETING INTERESTS STATEMENT**

671 The authors declare no competing interests.

672

673 **ACKNOWLEDGEMENTS**

674 We thank the flow cytometry and genomics staff at the Bauer Core Facility of Harvard University
675 Faculty of Arts and Sciences for advice on FACS sorting and sequencing, and members of the
676 Extavour lab for helpful discussions. This work was supported by NIH R01 award R01-HD073499-
677 0 to CGE, by funds from Harvard University, and by the Google Cloud Academic Research Credits
678 Program. CGE is a Howard Hughes Medical Institute investigator.

679

680 **AUTHOR CONTRIBUTIONS**

681 ST performed all steps in generating individual transcriptome datasets, including experimental
682 design, ovary dissection and dissociation, RNA-Seq library preparation and sequencing. GY
683 performed all statistical and network analyses of transcriptome data. TK performed and analysed
684 genetic experiments testing the role of *chinmo*. CGE conceived of the project, provided oversight
685 and funding. All authors drafted and edited the manuscript.

686

687 **DATA AVAILABILITY**

688 All the raw data are publicly available at NCBI-Gene Expression Omnibus (GEO) database under
689 the accession code GSE250320. Control datasets for early, mid and late-stage germ line and
690 somatic cells are accessible as a part of the NCBI-GEO database under the accession code
691 GSE172015 (GSM5239772-89). The scripts used to process and analyze the data are available
692 at the GitHub repository https://github.com/guillemylla/Ovariole_morphogenesis_RNAseq,
693 commit ID 171064d.

694 **REFERENCES**

695

696 Barolo S, Carver LA, Posakony JW. 2000. GFP and -Galactosidase Transformation Vectors for
697 Promoter/Enhancer Analysis in Drosophila. *BioTechniques* **29**: 726–732.

698 Barresi MJF, Gilbert SF. 2023. Developmental Biology.

699 Besse F, Busson D, Pret A. 2005. Hedgehog signaling controls Soma-Germen interactions
700 during Drosophila ovarian morphogenesis. *Dev Dynam* **234**: 422–431.

701 Brand AH, Perrimon N. 1993. Targeted gene expression as a means of altering cell fates and
702 generating dominant phenotypes. *Development* **118**: 401–415.

703 Büning J. 1994. Chapter 3. In *The Insect Ovary, Ultrastructure, previtellogenic growth and*
704 *evolution*, pp. 31–324.

705 Carlson M. 2024. AnnotationDbi: Introduction To Bioconductor Annotation Packages.
706 https://bioconductor.org/packages/release/bioc/html/AnnotationDbi.html.

707 Chen H-M, Marques JG, Sugino K, Wei D, Miyares RL, Lee T. 2020. CAMIO: a transgenic
708 CRISPR pipeline to create diverse targeted genome deletions in Drosophila. *Nucleic Acids*
709 *Res* **48**: 4344–4356.

710 Church SH, Medeiros BAS de, Donoughe S, Reyes NLM, Extavour CG. 2021. Repeated loss of
711 variation in insect ovary morphology highlights the role of development in life-history
712 evolution. *Proc Royal Soc B* **288**: 20210150.

713 David J. 1970. Le nombre d'ovarioles chez Drosophila melanogaster: relation avec la fécondité
714 et valeur adaptative. *Achives de Zoologie experimentale et generale* **111**: 357–370.

715 Dobin A, Davis CA, Schlesinger F, Drenkow J, Zaleski C, Jha S, Batut P, Chaisson M, Gingeras
716 TR. 2013. STAR: ultrafast universal RNA-seq aligner. *Bioinformatics* **29**: 15–21.

717 Dong J, Feldmann G, Huang J, Wu S, Zhang N, Comerford SA, Gayyed MF, Anders RA, Maitra
718 A, Pan D. 2007. Elucidation of a Universal Size-Control Mechanism in Drosophila and
719 Mammals. *Cell* **130**: 1120–1133.

720 Enomoto M, Takemoto D, Igaki T. 2021. Interaction between Ras and Src clones causes
721 interdependent tumor malignancy via Notch signaling in Drosophila. *Dev Cell* **56**: 2223-
722 2236.e5.

723 Extavour CGM. 2007. Gray anatomy: phylogenetic patterns of somatic gonad structures and
724 reproductive strategies across the Bilateria. *Integr Comp Biol* **47**: 420–426.

725 Fisher KH, Wright VM, Taylor A, Zeidler MP, Brown S. 2012. Advances in genome-wide RNAi
726 cellular screens: a case study using the Drosophila JAK/STAT pathway. *BMC Genom* **13**:
727 506.

728 Flaherty MS, Zavadil J, Ekas LA, Bach EA. 2009. Genome-wide expression profiling in the
729 Drosophila eye reveals unexpected repression of notch signaling by the JAK/STAT pathway.
730 *Dev Dyn* **238**: 2235–2253.

731 Godt D, Laski FA. 1995. Mechanisms of cell rearrangement and cell recruitment in Drosophila
732 ovary morphogenesis and the requirement of bric a brac. *Development* **121**: 173–187.

733 Grmai L, Harsh S, Lu S, Korman A, Deb IB, Bach EA. 2021. Transcriptomic analysis of
734 feminizing somatic stem cells in the Drosophila testis reveal putative downstream effectors of
735 the transcription factor Chinmo. *G3 Genes Genomes Genetics* **11**: jkab067-.

736 Hodin J. 2009. Chapter 11. She Shapes Events As They Come: Plasticity in Female Insect
737 Reproduction. In *Phenotypic Plasticity of Insects* (ed. D.W. Whitman).

738 Honěk A. 1993. Intraspecific Variation in Body Size and Fecundity in Insects: A General
739 Relationship. *Oikos* **66**: 483.

740 Huang J, Wu S, Barrera J, Matthews K, Pan D. 2005. The Hippo Signaling Pathway
741 Coordinately Regulates Cell Proliferation and Apoptosis by Inactivating Yorkie, the
742 Drosophila Homolog of YAP. *Cell* **122**: 421–434.

743 Kim-Ha J, Kerr K, Macdonald PM. 1995. Translational regulation of oskar mRNA by Bruno, an
744 ovarian RNA-binding protein, is essential. *Cell* **81**: 403–412.

745 King R. 1970. *Ovarian Development in Drosophila Melanogaster*. Academic Press.

746 King RC, Aggarwal SK, Aggarwal U. 1968. The development of the female Drosophila
747 reproductive system. *J Morphol* **124**: 143–165.

748 Kumar T, Blondel L, Extavour CG. 2020. Topology-driven protein-protein interaction network
749 analysis detects genetic sub-networks regulating reproductive capacity. *Elife* **9**: e54082.

750 Larkin A, Marygold SJ, Antonazzo G, Attrill H, dos Santos G, Garapati PV, Goodman JL,
751 Gramates LS, Millburn G, Strelets VB, et al. 2020. FlyBase: updates to the Drosophila
752 melanogaster knowledge base. *Nucleic Acids Res* **49**: D899–D907.

753 Lasko PF, Ashburner M. 1988. The product of the Drosophila gene vasa is very similar to
754 eukaryotic initiation factor-4A. *Nature* **335**: 611–617.

755 Li B, Dewey CN. 2011. RSEM: accurate transcript quantification from RNA-Seq data with or
756 without a reference genome. *BMC Bioinform* **12**: 323.

757 Li MA, Alls JD, Avancini RM, Koo K, Godt D. 2003. The large Maf factor Traffic Jam controls
758 gonad morphogenesis in Drosophila. *Nat Cell Biol* **5**: 994–1000.

759 Lindsley DL, Grell EH. 1968. *Genetic Variations of Drosophila melanogaster*. Carnegie
760 Institution of Washington, Washington, DC, USA.

761 Love MI, Huber W, Anders S. 2014. Moderated estimation of fold change and dispersion for
762 RNA-seq data with DESeq2. *Genome Biol* **15**: 550.

763 Ma Q, Cuevas M de, Matunis EL. 2016. Chinmo is sufficient to induce male fate in somatic cells
764 of the adult Drosophila ovary. *Development* **143**: 754–763.

765 Manning SA, Kroeger B, Deng Q, Brooks E, Fonseka Y, Hinde E, Harvey KF. 2024. The
766 Drosophila Hippo pathway transcription factor Scalloped and its co-factors alter each other's
767 chromatin binding dynamics and transcription in vivo. *Dev Cell* **59**: 1640-1654.e5.

768 Markow TA, O'Grady PM. 2007. Drosophila Biology in the Genomic Age. *Genetics* **177**: 1269–
769 1276.

770 Matsuoka S, Hiromi Y, Asaoka M. 2013. Egfr signaling controls the size of the stem cell
771 precursor pool in the Drosophila ovary. *Mech Dev* **130**: 241–253.

772 Moon S, Kim W, Kim S, Kim Y, Song Y, Bilousov O, Kim J, Lee T, Cha B, Kim M, et al. 2017.
773 Phosphorylation by NLK inhibits YAP-14-3-3-interactions and induces its nuclear localization.
774 *EMBO Rep* **18**: 61–71.

775 Murali T, Pacifico S, Yu J, Guest S, Roberts GG, Finley RL. 2011. DroID 2011: a
776 comprehensive, integrated resource for protein, transcription factor, RNA and gene
777 interactions for Drosophila. *Nucleic Acids Res* **39**: D736–D743.

778 Nadimpalli S, Persikov AV, Singh M. 2015. Pervasive Variation of Transcription Factor
779 Orthologs Contributes to Regulatory Network Evolution. *PLoS Genet* **11**: e1005011.

780 Oh H, Irvine KD. 2008. In vivo regulation of Yorkie phosphorylation and localization.
781 *Development* **135**: 1081–1088.

782 Oh H, Slattery M, Ma L, Crofts A, White KP, Mann RS, Irvine KD. 2013. Genome-wide
783 Association of Yorkie with Chromatin and Chromatin-Remodeling Complexes. *Cell Rep* **3**:
784 309–318.

785 Oh H, Slattery M, Ma L, White KP, Mann RS, Irvine KD. 2014. Yorkie Promotes Transcription by
786 Recruiting a Histone Methyltransferase Complex. *Cell Rep* **8**: 449–459.

787 Rust K, Byrnes LE, Yu KS, Park JS, Sneddon JB, Tward AD, Nystul TG. 2020. A single-cell
788 atlas and lineage analysis of the adult Drosophila ovary. *Nat Commun* **11**: 5628.

789 Sarikaya DP, Belay AA, Ahuja A, Dorta A, Green DA, Extavour CG. 2012. The roles of cell size
790 and cell number in determining ovariole number in Drosophila. *Dev Biol* **363**: 279–289.

791 Sarikaya DP, Extavour CG. 2015. The Hippo Pathway Regulates Homeostatic Growth of Stem
792 Cell Niche Precursors in the Drosophila Ovary. *Plos Genet* **11**: e1004962.

793 Schindelin J, Arganda-Carreras I, Frise E, Kaynig V, Longair M, Pietzsch T, Preibisch S,
794 Rueden C, Saalfeld S, Schmid B, et al. 2012. Fiji: an open-source platform for biological-
795 image analysis. *Nat Methods* **9**: 676–82.

796 Slattery M, Voutev R, Ma L, Nègre N, White KP, Mann RS. 2013. Divergent Transcriptional
797 Regulatory Logic at the Intersection of Tissue Growth and Developmental Patterning. *PLoS*
798 *Genet* **9**: e1003753.

799 Song X, Call GB, Kirilly D, Xie T. 2007. Notch signaling controls germline stem cell niche
800 formation in the Drosophila ovary. *Development* **134**: 1071–1080.

801 Spokony RF, Restifo LL. 2007. Anciently duplicated Broad Complex exons have distinct
802 temporal functions during tissue morphogenesis. *Dev Genes Evol* **217**: 499–513.

803 Tapon N, Harvey KF, Bell DW, Wahrer DCR, Schiripo TA, Haber DA, Hariharan IK. 2002.
804 salvador Promotes Both Cell Cycle Exit and Apoptosis in Drosophila and Is Mutated in
805 Human Cancer Cell Lines. *Cell* **110**: 467–478.

806 Tarikere S, Ylla G, Extavour CG. 2021. Distinct gene expression dynamics in germ line and
807 somatic tissue during ovariole morphogenesis in Drosophila melanogaster. *G3 Genes*
808 *Genomes Genetics*.

809 Tinevez J-Y, Perry N, Schindelin J, Hoopes GM, Reynolds GD, Laplantine E, Bednarek SY,
810 Shorte SL, Eliceiri KW. 2017. TrackMate: An open and extensible platform for single-particle
811 tracking. *Methods* **115**: 80–90.

812 Wang H, Chen X, He T, Zhou Y, Luo H. 2013. Evidence for Tissue-Specific JAK/STAT Target
813 Genes in Drosophila Optic Lobe Development. *Genetics* **195**: 1291–1306.

814 Wang W, Xiao Z-D, Li X, Aziz KE, Gan B, Johnson RL, Chen J. 2015. AMPK modulates Hippo
815 pathway activity to regulate energy homeostasis. *Nat Cell Biol* **17**: 490–499.

816 Wu S, Huang J, Dong J, Pan D. 2003. hippo Encodes a Ste-20 Family Protein Kinase that
817 Restricts Cell Proliferation and Promotes Apoptosis in Conjunction with salvador and warts.
818 *Cell* **114**: 445–456.

819 Wu S, Liu Y, Zheng Y, Dong J, Pan D. 2008. The TEAD/TEF Family Protein Scalloped
820 Mediates Transcriptional Output of the Hippo Growth-Regulatory Pathway. *Dev Cell* **14**: 388–
821 398.

822 Xu T, Wang W, Zhang S, Stewart RA, Yu W. 1995. Identifying tumor suppressors in genetic
823 mosaics: the Drosophila lats gene encodes a putative protein kinase. *Development* **121**:
824 1053–1063.

825 Yatsenko AS, Shcherbata HR. 2021. Distant activation of Notch signaling induces stem cell
826 niche assembly. *Plos Genet* **17**: e1009489.

827 Yu G, Wang L-G, Han Y, He Q-Y. 2012. clusterProfiler: an R Package for Comparing Biological
828 Themes Among Gene Clusters. *OMICS: A J Integr Biol* **16**: 284–287.

829 Yu J, Pacifico S, Liu G, Finley RL. 2008. DroID: the Drosophila Interactions Database, a
830 comprehensive resource for annotated gene and protein interactions. *BMC Genom* **9**: 461.

831 Zhang L, Ren F, Zhang Q, Chen Y, Wang B, Jiang J. 2008. The TEAD/TEF Family of
832 Transcription Factor Scalloped Mediates Hippo Signaling in Organ Size Control. *Dev Cell* **14**:
833 377–387.

834 Zhao B, Wei X, Li W, Udan RS, Yang Q, Kim J, Xie J, Ikenoue T, Yu J, Li L, et al. 2007.
835 Inactivation of YAP oncoprotein by the Hippo pathway is involved in cell contact inhibition
836 and tissue growth control. *Genes Dev* **21**: 2747–2761.

837 Zhao B, Ye X, Yu J, Li L, Li W, Li S, Yu J, Lin JD, Wang C-Y, Chinnaiyan AM, et al. 2008. TEAD
838 mediates YAP-dependent gene induction and growth control. *Gene Dev* **22**: 1962–1971.

839 Zheng Y, Pan D. 2019. The Hippo Signaling Pathway in Development and Disease. *Dev Cell*
840 **50**: 264–282.

841 Zhu S, Lin S, Kao C-F, Awasaki T, Chiang A-S, Lee T. 2006. Gradients of the Drosophila
842 Chinmo BTB-Zinc Finger Protein Govern Neuronal Temporal Identity. *Cell* **127**: 409–422.

843

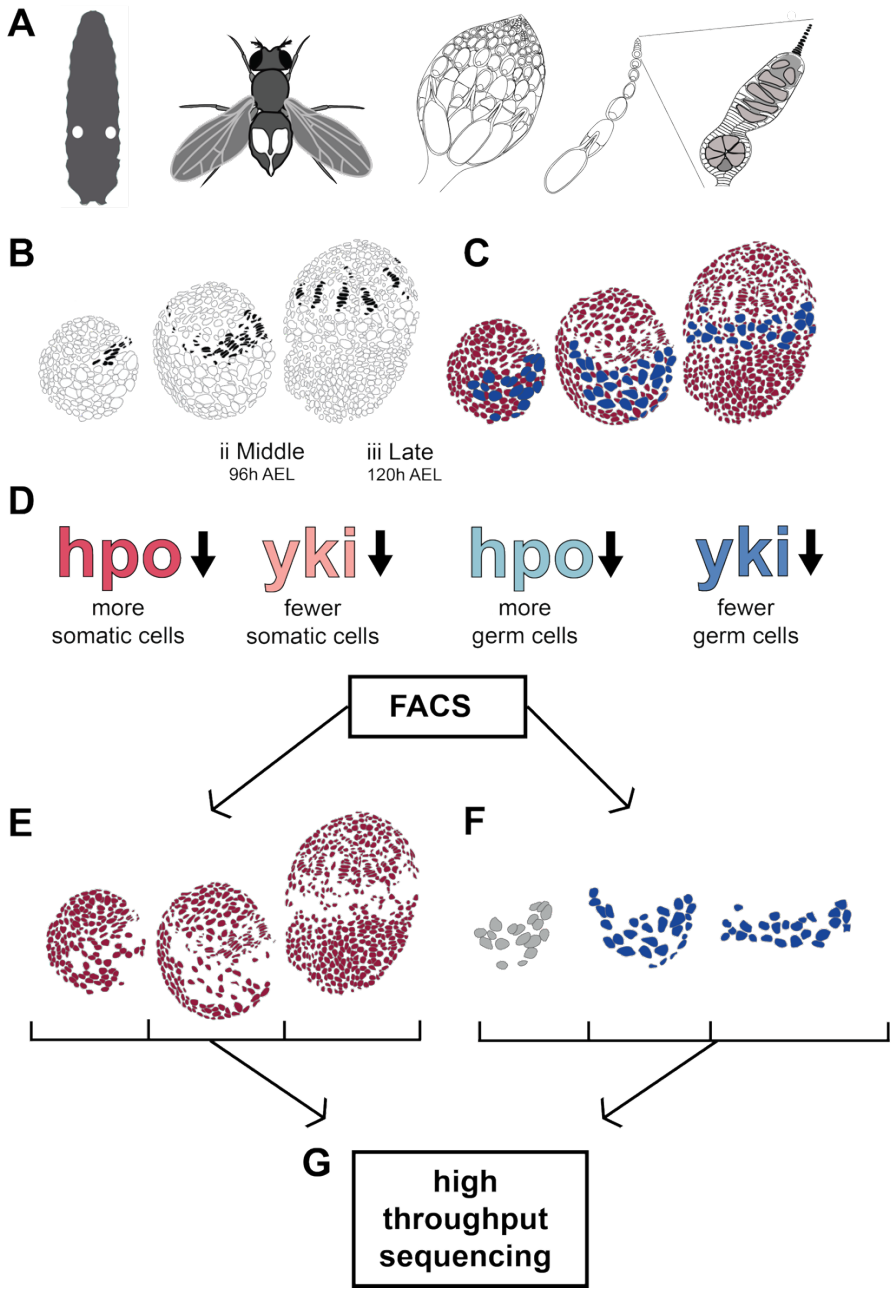

Figure 1: Experimental design to generate stage-specific transcriptomes of in somatic and germ line larval ovarian cells under wild type, *hpo* and *yki* loss of function conditions. (A) Left to right: Location of larval ovaries (indicated as white circles in the larva); location of adult ovaries in female abdomen (indicated in white within the abdomen); a single adult ovary; a single ovariole; a single germarium with terminal filaments in black. **(B)** The three developmental stages during terminal filament (in black) formation studied herein. **(C)** Somatic (red) and germ line (blue) cells were marked for FACS sorting using appropriate GAL4 drivers as described in Materials & Methods. **(D)** Summary of the tissue-specific RNAi knockdown treatments assessed at each stage in somatic and germ line cells. GFP labelled somatic cells **(E)** and germ cells **(F)** were sorted using FACS at the three developing stages of larval ovaries. Data from early-stage germ cells (grey), were not used for analysis; see Materials & Methods. **(G)** Sorted ovarian cell types were processed for mRNA extraction, cDNA library preparation and high throughput sequencing. h AEL = hours after egg laying.

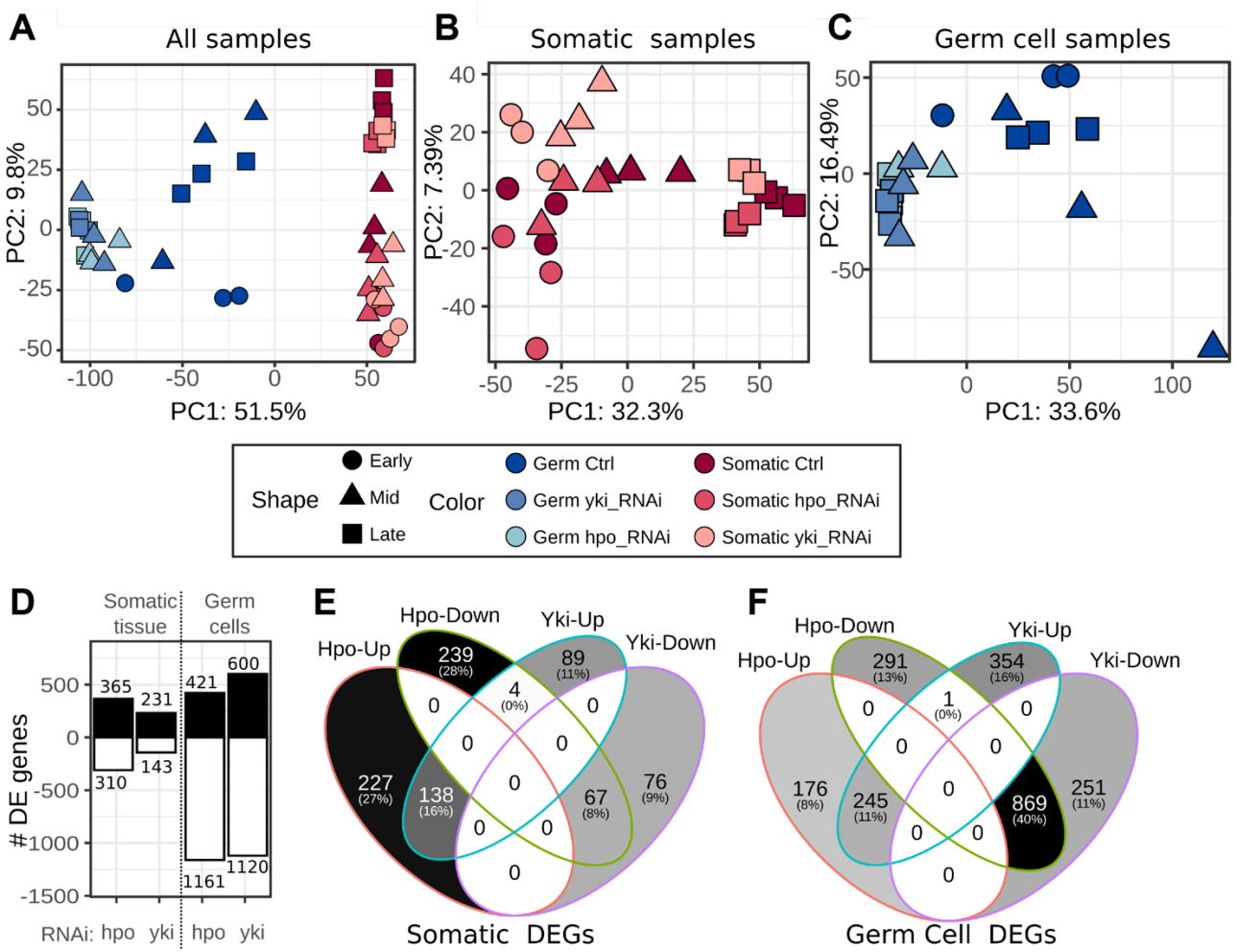

Figure 2: Distinct transcriptional impact of Hpo signaling on germ line and soma across ovarian development . (A) Principal Component Analysis (PCA) of all samples differentiates germ cells from somatic cells along PC1. (B) PCA of somatic transcriptomes showing clustering by time-point in PC1, and the knockdown effect in PC2. **(C)** PCA of germ line transcriptomes in which control and knockdown libraries cluster separately, but the *hpo* and *yki* knockdowns cluster together. **(D)** Number of significantly upregulated and downregulated genes (adjusted p-value < 0.05) in each cell type with grouped stages when comparing each knockdown to the control library. For somatic cells **(E)** and germ cells **(F)** a Venn diagram shows the differentially up- and down- regulated genes under each knockdown, including number and percentage of genes in each intersection.

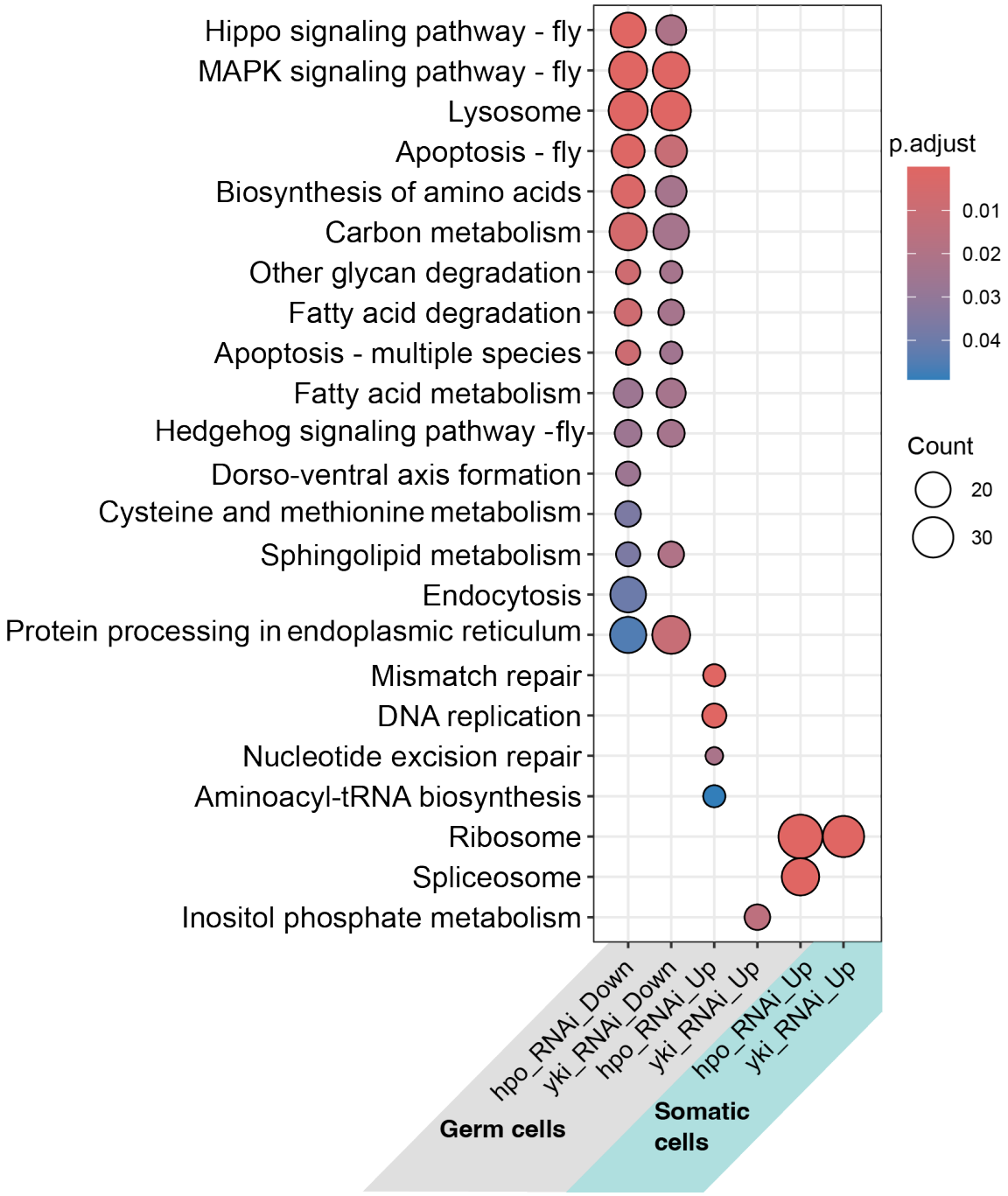

Figure 3: Perturbing *hpo* or *yki* levels has a larger transcriptomic impact on germ cells than somatic cells. Shown are significantly enriched (Benjamini-Hochberg adjusted p-value<0.05) KEGG pathways within the groups of significantly upregulated (Up) and downregulated (Down) genes in germ cells and somatic cells under *hpo* and *yki* RNAi conditions (grouping mid and late stages together).

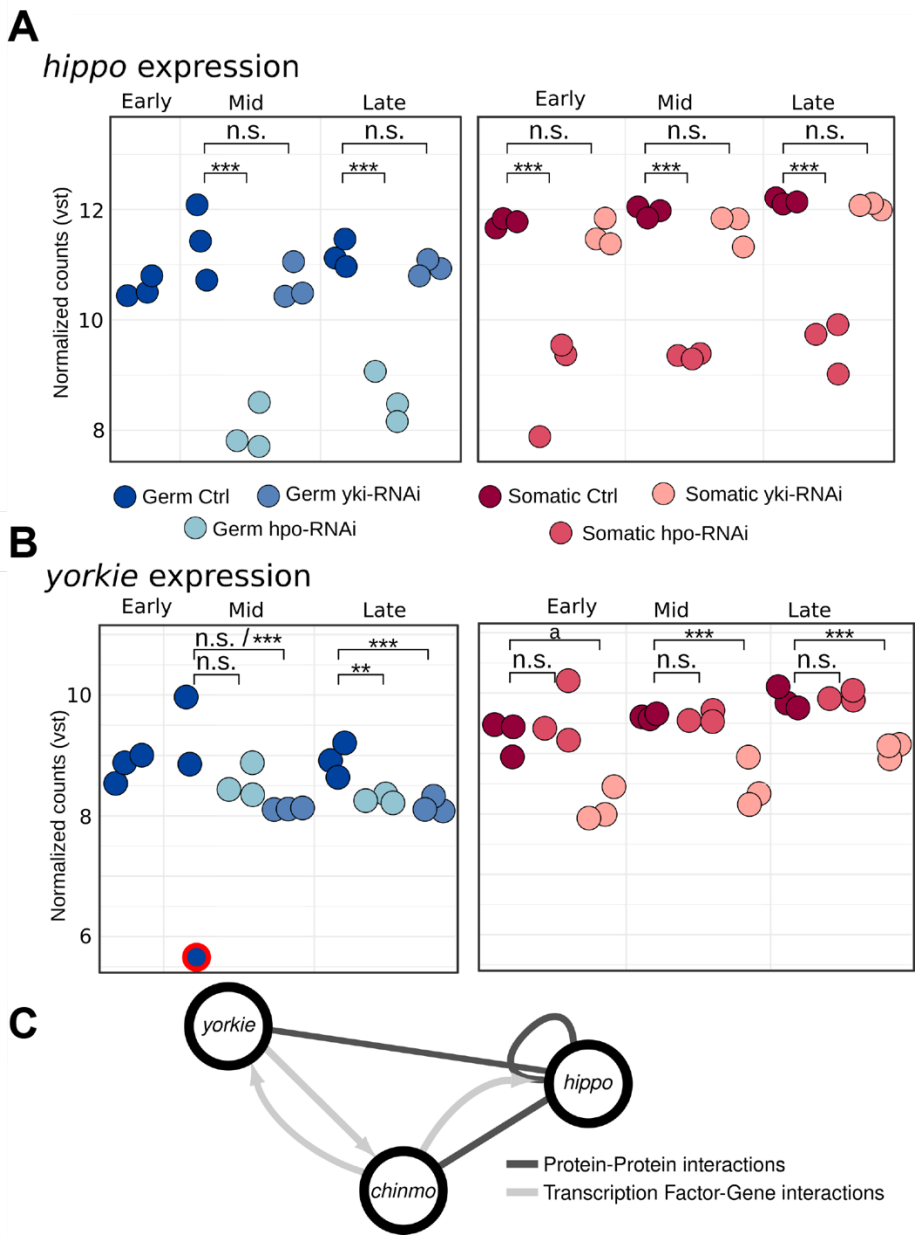

Figure 4: Prediction of chinmo as a novel germ cell-specific candidate regulator of *hpo* and/or *yki*. Expression of **(A)** *hpo* and **(B)** *yki* as vst-normalized counts in germ cells (left panels, blue dots) and somatic cells (right panels, red dots) in each RNA-Seq library (color shades indicate genetic condition). The *hpo* and *yki* transcripts appear significantly downregulated their corresponding RNAi conditions. The *yki* reduction in germ cells mid stages is significant when the control sample with anomalously low levels of *yki* (circled in red) is removed (Supplemental Figure S3). Additionally, *yki* appears significantly downregulated under *hpo* knockdown. Statistical significance levels from the differential expression analysis are codified as *** = adjusted p-value<0.01; ** = adjusted p-value<0.05; [a] = adjusted p-value = 0.055, n.s. = not significant. **(C)** Graph showing *hpo*, *yki*, and their only common direct neighbor in our network of protein-protein interactions, *chinmo*. Protein-protein candidate interaction edges are represented in dark grey, and transcription factor-gene candidate interactions are represented in light grey arrows with pointing to the gene predicted to be regulated by the TF. The TF *chinmo* appears has the potential to regulate both *hpo* and *yki*, can physically interact with *hpo*, and can potentially be regulated by *yki*.

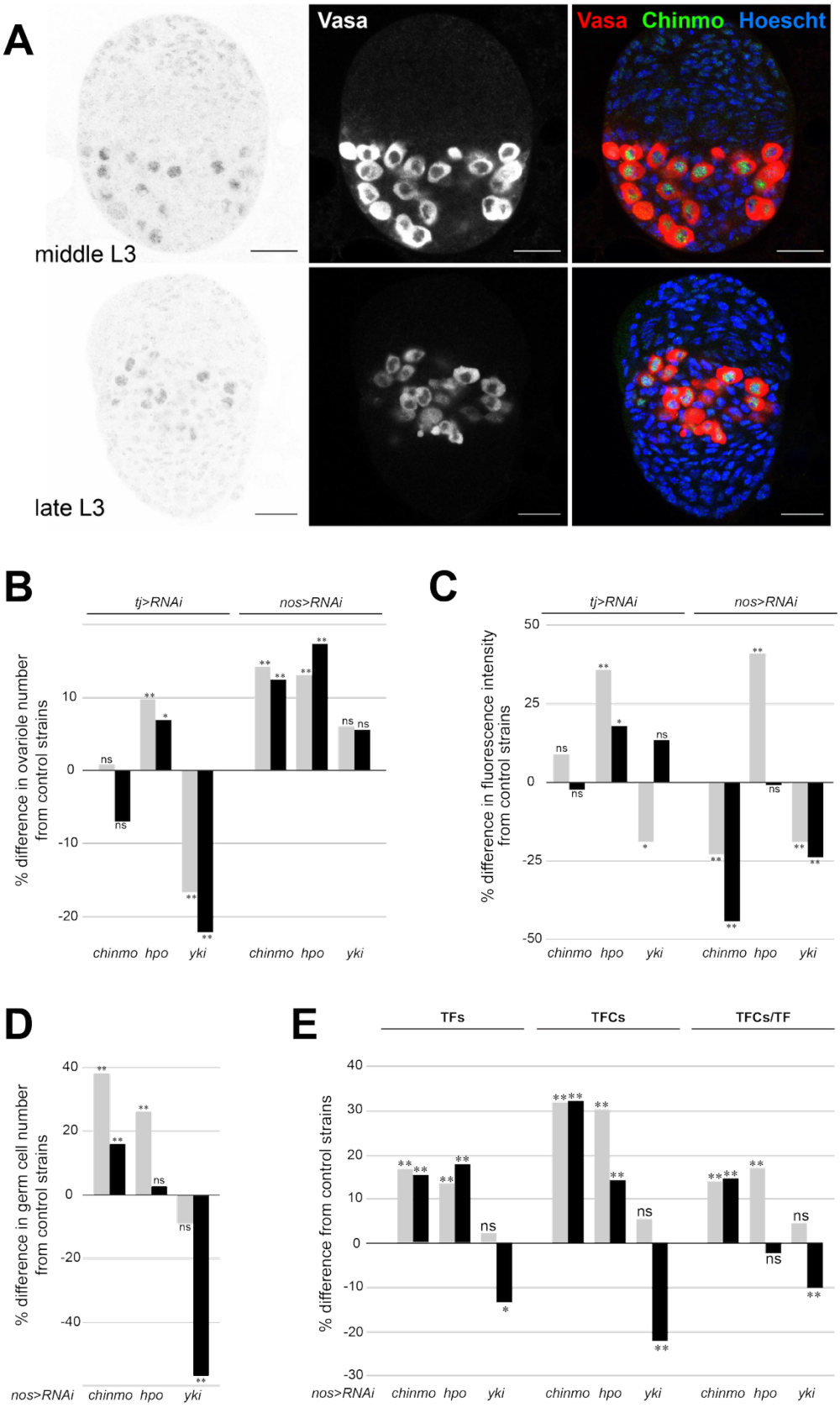
A
Vasa
Vasa Chinmo Hoescht
middle L3
late L3
B
tj>RNAi
nos>RNAi
% difference in ovariole number from control strains
chinmo hpo yki chinmo hpo yki
C
tj>RNAi
nos>RNAi
% difference in fluorescence intensity from control strains
chinmo hpo yki chinmo hpo yki
D
% difference in germ cell number from control strains
nos>RNAi chinmo hpo yki
E
TFs
TFCs
TFCs/TF
% difference from control strains
nos>RNAi chinmo hpo yki chinmo hpo yki chinmo hpo yki

885

886 **Figure 5: Chinmo regulates germ cell number autonomously and somatic cell number and**
887 **morphogenesis non-autonomously in the developing ovary. (A)** Chinmo is detected in germ cell
888 nuclei at mid and late stages of larval development. Red = Vasa; Chinmo = green, scale bars = 20μm.
889 **(B)** *chinmo RNAi* in the germ cells causes an increase in ovariole number. Percentage difference in
890 adult ovariole number where *UAS:chinmo [RNAi]*, *UAS:hippo [RNAi],* or *UAS:yorkie [RNAi]* are driven
891 in the somatic cells or in the germ cells. n=20 for each genotype. **(C)** Abrogation of Hpo signaling in
892 the germ cells causes a change in Chinmo levels in germ cell nuclei. Percentage difference in detected
893 fluorescence levels of Chinmo protein in larval ovarian germ cell nuclei where *UAS:chinmo [RNAi]*,
894 *UAS:hippo [RNAi]* or *UAS:yorkie [RNAi]* are driven in the somatic cells in the germ cells. $n \geq 50$ nuclei
895 from five ovaries. **(D)** *chinmo RNAi* in germ cells causes an increase in germ cell number. Percentage
896 difference in germ cell number where *UAS:chinmo [RNAi]*, *UAS:hippo [RNAi]* or *UAS:yorkie [RNAi]*
897 are driven in germ cells. **(E)** *chinmo* RNAi in germ cells causes an increase in Terminal Filament (TF)
898 number, Total Terminal Filament Cell (TFC) number and in the number of TFCs per TF. Percentage
899 differences in TF number and TFC number in each ovary, and the number of TFCs per TF where
900 *UAS:chinmo [RNAi]*, *UAS:hippo [RNAi]* or *UAS:yorkie [RNAi]* were driven in the germ cells. In **B**
901 through **E**, grey bars = comparisons to *Gal4* controls; blacks bars = comparisons to *UAS* controls.
902 Statistical significance was calculated using a student's two-tailed t-test with unequal variance. (** =
903 $p<0.01$, * = $p<0.05$, ns = $p>0.05$).

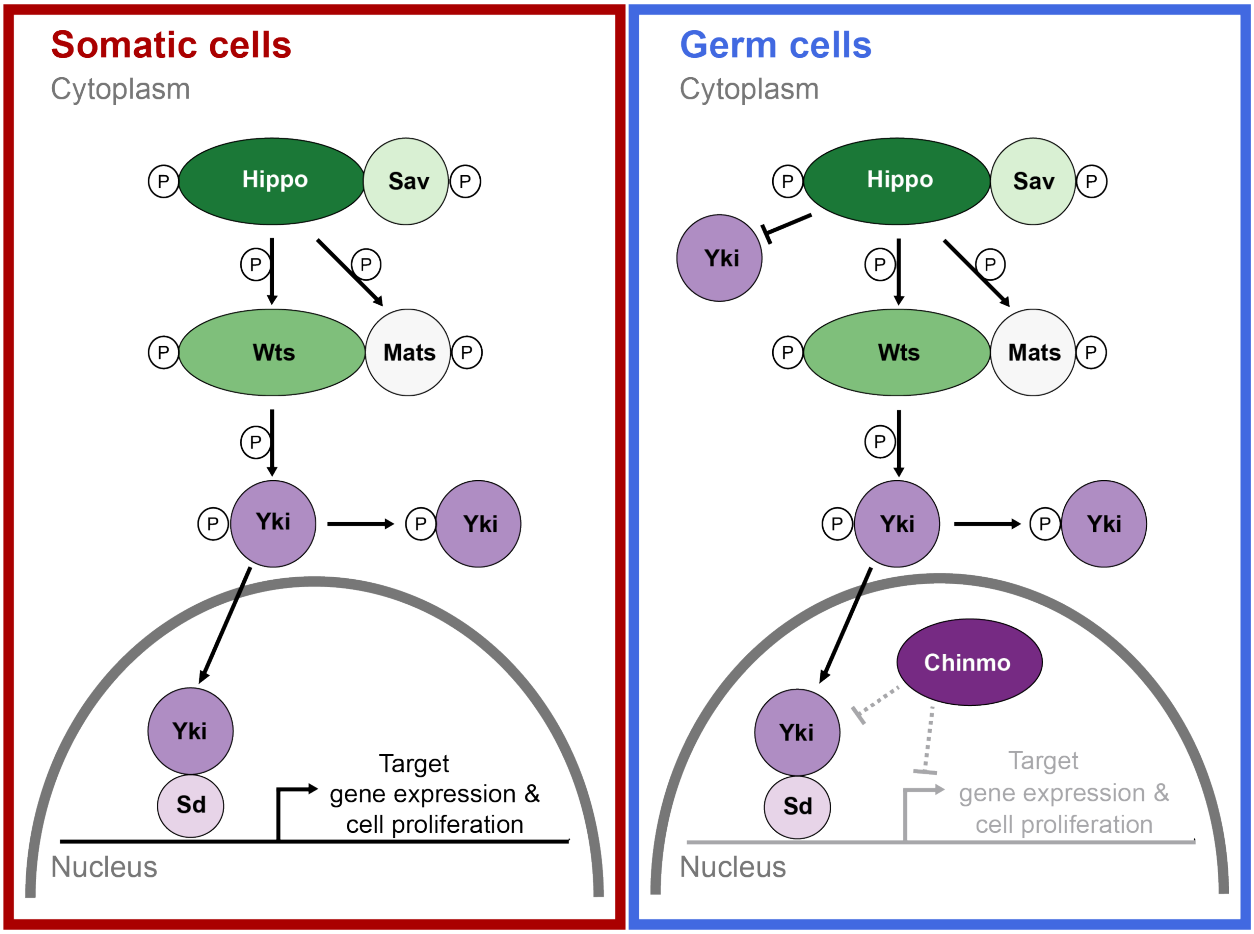

Figure 6. Hypothesis: Chinmo regulates Hpo signaling activity in the germ cells but not somatic cells. We previously showed that the components of the Hippo signaling pathway are present in both the germ and somatic cells, (Sarikaya 2015), and that the somatic cells (red) function under the influence of the canonical Hippo pathway (Sarikaya 2015). Under this model, the reduction of either *hpo* or *yki* causes a change in germ cell number. In germ cells (blue), Chinmo is present, which adds a secondary Hippo-independent repression of *yki*-dependent cell proliferation. Because our data cannot determine whether Chinmo acts directly on the localization of Yki to the nucleus, or indirectly by repressing cell proliferation downstream of Yki, the Chinmo-Yki relationship is indicated by grey dashed lines.